Electron standing waves on the Si(111)- $\sqrt{3} \times \sqrt{3}$-Ag surface

Norio Sato and Sakura Takeda

Department of Physics, School of Science, University of Tokyo, 7-3-1 Hongo Bunkyo-ku, Tokyo 113-0033, Japan

Tadaaki Nagao and Shuji Hasegawa

Department of Physics, School of Science, University of Tokyo, 7-3-1 Hongo Bunkyo-ku, Tokyo 113-0033, Japan
and Core Research for Evolutional Science and Technology, The Japan Science and Technology Corporation,
Kawaguchi Center Building, Hon-cho 4-1-8, Kawaguchi, Saitama 332-0012, Japan

Electron standing waves have been observed near step edges and out-of-phase domain boundaries on the Si(111)-$\sqrt{3} \times \sqrt{3}$-Ag surface using scanning tunneling microscopy at 6 K. This means that this surface has a two-dimensional free-electron-like surface electronic state. Their wavelengths change with the bias voltages, so that the dispersion relations between energy and wave number have been obtained. We have found two types of out-of-phase domain boundaries of the $\sqrt{3} \times \sqrt{3}$-Ag structure, one of which acts as a potential barrier for the surface-state electrons to make the standing waves, while the other type does not. [S0163-1829(99)00203-9]

Electron standing waves on surfaces are oscillatory spatial modulations of local density of states caused by localized scattering potentials such as atomic step edges and adsorbed foreign atoms. These waves are observed by scanning tunneling microscopy (STM) on noble metal surfaces,[1–3] and Be surface,[4] where free-electron-like surface electronic states exist. That is, parabolic surface-state bands crossing the Fermi level (E_F) exist, meaning also a metallic nature. So the wavelength of the standing waves with low-bias voltages (probing only the states near E_F) is equal to half of the Fermi wavelength. These waves are also called energy-resolved Friedel oscillations. Adding to these measurements in two-dimensional surface states, Friedel oscillations in bulk states caused by substances in the subsurface region have been also observed on Al surface[5] and GaAs surface.[6]

On the other hand, for the Si(111)-$\sqrt{3} \times \sqrt{3}$-Ag surface, a honeycomb-chained-trimer (HCT) model is now widely accepted as its atomic arrangement.[7,8] Based on this model, surface electronic states are calculated, which shows a Γ-centered free-electron-like band.[9] Actually, this band has been detected by photoemission spectroscopy.[10–12]

In this paper, we present STM observations of electron standing waves formed on the $\sqrt{3} \times \sqrt{3}$-Ag surface at 6 K using ultrahigh vacuum scanning tunneling microscopy. As far as we know, this is the first time that electron standing waves due to a surface-state band on the semiconductor with superlattice structures have been observed. The standing waves were found at particular out-of-phase domain boundaries of the $\sqrt{3} \times \sqrt{3}$-Ag superstructures as well as step edges. Their wavelengths were also found to change with bias voltages, so that the dispersion relations between energy and wave number were extracted from those images.

We used a commercial ultrahigh vacuum low-temperature STM (UNISOKU USM501 type) equipped with reflection high-energy electron diffraction (RHEED) system for preparing sample surfaces. This STM can operate at low temperatures down to 6 K. The base pressure in the chambers was less than 1×10^{-10} Torr. The substrate was a p-type Si(111)

wafer with 0.01 Ω cm resistivity at RT and about ten times higher at 6 K. Its dimension was $14 \times 2 \times 0.4$ mm^3. It was clamped to a holder with Mo plates. An electrochemically etched polycrystalline W tip was used.

A clear Si(111)-7×7 RHEED pattern was produced by flashing the sample at 1200 °C several times. The $\sqrt{3} \times \sqrt{3}$-Ag structure was prepared by depositing about 1 ML of Ag with a rate of 0.014 ML/sec on the 7×7 surface kept at 500 °C. The surface structure was always monitored by RHEED during Ag deposition. After this preparation, the sample was cooled down to 6 K on the STM stage.

A typical image taken in constant-height mode is shown in Fig. 1 (650 Å×610 Å). In our constant-height mode, slow feed back with a large time constant was applied. So, on flat terraces, the image is almost the same as a true constant-height-mode STM image without feed back. But at the steps or domain boundaries, the height difference is stressed. The sample bias voltage is 0.75 V, probing the empty states. A 7×7 domain is seen at the upper-right corner in the image. The rest of the surface is the $\sqrt{3} \times \sqrt{3}$-Ag structure, where fine periodic corrugations are seen. One can also see the standing wave patterns superimposed near step edges in the $\sqrt{3} \times \sqrt{3}$-Ag area. Its wavelength is about 25 Å. On the circular domain in the upper part of the image, a complicated interference pattern is observed. Near the step edges at the lower left, standing wave patterns are parallel to the step edge. In the filled-state images, we could not obtain any standing wave patterns.

Figure 1(b) is a Fourier transformed pattern of a square area indicated in Fig. 1(a). Hexagonal spots (indicated by A) in this pattern correspond to the $\sqrt{3} \times \sqrt{3}$ periodicity in the real-space image of Fig. 1(a). We have a ring (indicated by B) near the center spot which comes from the standing waves. Its radius, which is equal to twice the wave number of the standing wave pattern, is about 0.26 Å^{-1}.

The same area was scanned with different bias voltages. In Fig. 2, as the positive sample bias voltage was decreased, the wavelength of the standing waves became longer. From
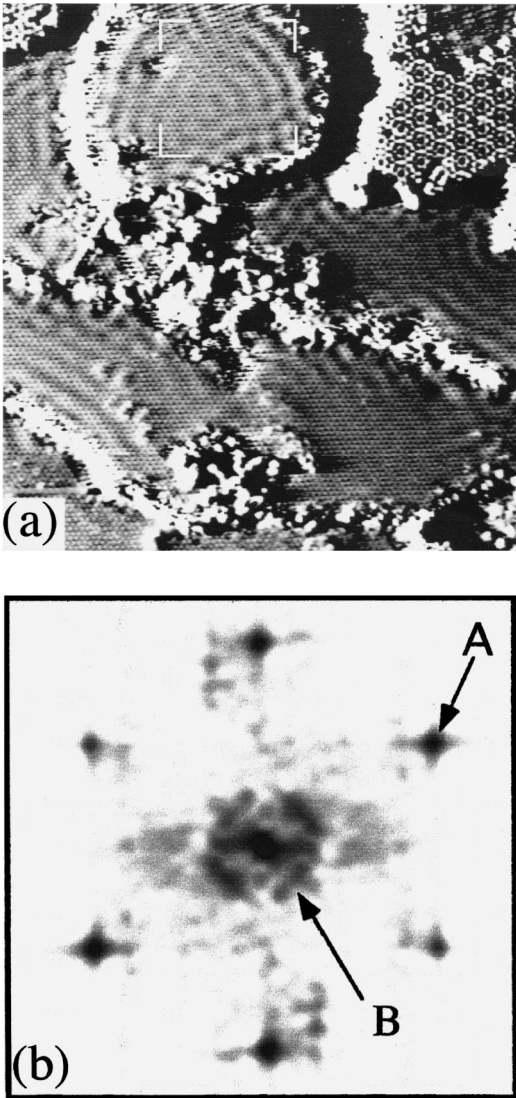
FIG. 1. (a) An STM image with electron standing wave patterns on Si(111)-$\sqrt{3} \times \sqrt{3}$-Ag surface. The size is 650 Å×610 Å. The tunneling current is 0.5 nA with sample bias voltage of 0.75 V. The defective areas in the center of the image may be amorphous Si, which was made by repeating the flash heating around the temperature as high as the melting point of Si. (b) A two-dimensional fast Fourier transformed pattern of the square area (160 Å×160 Å) indicated in (a). The distance between the center spot and the hexagonal spots A (corresponding to the $\sqrt{3} \times \sqrt{3}$ diffraction spots) is 1.1 Å^{-1}.

these images, we got the dispersion relations between energy E and wave number k as described below.

We observed standing waves also near out-of-phase boundaries (OPB's) of the $\sqrt{3} \times \sqrt{3}$-Ag domains[13–16] as shown in Fig. 3. The difference of two types of OPB's seen in Fig. 3 will be discussed later. The wavelength of the standing waves near the straight OPB also changed depending on the bias voltage. Some of the profiles of the waves as a function of the distance away from the OPB along the direction perpendicular to the OPB are shown in Fig. 4(a). By laterally averaging such profiles at each bias voltage and measuring the distance of the peak positions, the wavelengths of the standing waves were obtained as a function of
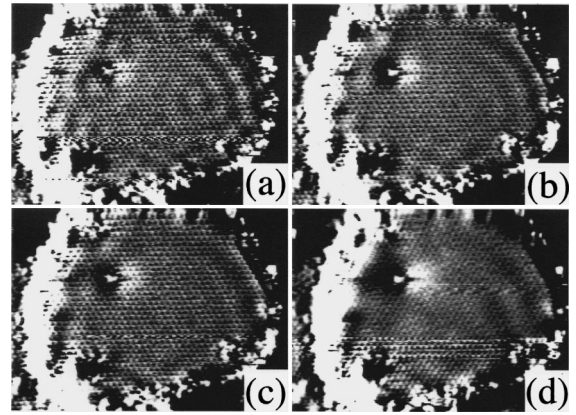
FIG. 2. Empty-state STM images (265 Å×330 Å) on the same surface as Fig. 1(a) with different bias voltages, (a) 0.6 V, (b) 0.5 V, (c) 0.4 V, and (d) 0.3 V with a constant tunneling current of 0.5 nA.

the bias voltage, which are shown in Fig. 4(b) with closed squares.

The dispersion relation at the circular domain in Fig. 2 is also shown in Fig. 4(b) with closed triangles. The data set in Fig. 4(b) with closed circles is obtained near another OPB.

Though the theoretical calculation[9] shows that the bands are anisotropic [shown in Fig. 4(b) with dashed curves], we assumed isotropic bands within the error of the ring in Fig. 1(b). A parabola ($E = \hbar^2 k^2 / 2m^* + \text{const}$, where $\hbar$ is Planck's constant, m^* an electron effective mass) was fitted to the experimental data. The validity of this fit by using the constant-height STM images will be discussed later. The bottom of the fitted parabola (obtained from the data set with closed triangles) at the $\bar{\Gamma}$ point is (0.06 ± 0.08) eV above E_F. m^* is $(0.10 \pm 0.04)m_e$, where m_e is the free-electron mass.

The effective masses m^* obtained from the standing waves near the straight out-of-phase boundaries were fairly reproducible, $(0.13 \pm 0.03)m_e$ and $(0.13 \pm 0.04)m_e$ (whose data sets are shown in Fig. 4(b) with closed squares and closed circles, respectively), which deviates substantially from the experimental data of photoemission spectroscopy $m^* = 0.25 m_e$ [closed diamonds in Fig. 4(b)],[10] while the
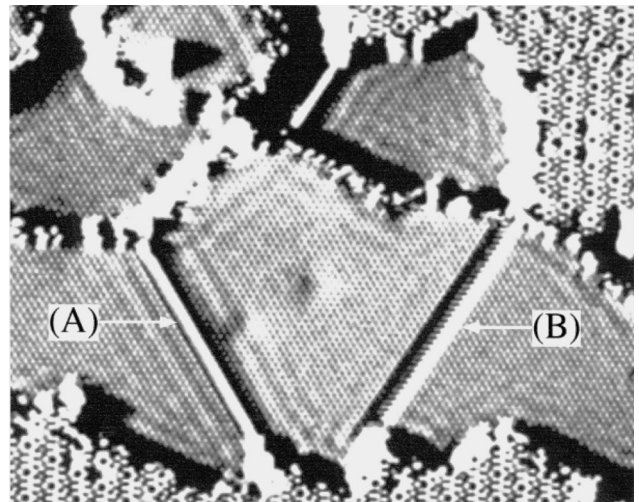
FIG. 3. An empty-state STM image (485 Å×645 Å) with the tunneling current of 0.18 nA, and the sample bias voltage 1.0 V.

(a)

(b)
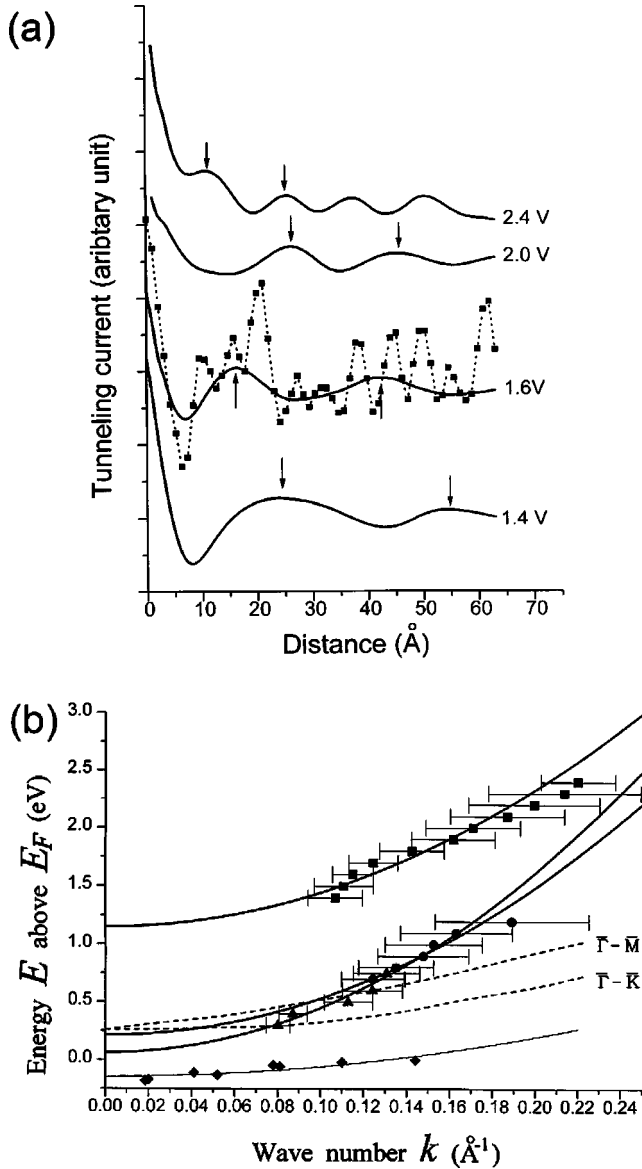
FIG. 4. (a) Profiles of the standing-wave pattern at different sample bias voltages as a function of the distance along the direction perpendicular to the straight OPB. The raw data (typically shown with the dotted curve superimposed on the solid curve at the bias voltage 1.6 V) are low-pass filtered and smoothed to get the solid curve. The arrows show the first peaks and second peaks used to estimate the wavelengths at each voltage. (b) Dispersion relations between wave number and energy of the standing waves with fitted parabolas. Solid squares, circles, and triangles are data taken from different samples cut from the same wafer. Dashed curves are the first-principle calculations taken from Ref. 9, and the thin solid curve with closed diamonds is obtained by the photoemission measurement taken from Ref. 10.

first-principle calculations[9] indicate $m^* = 0.4 m_e$ for the $\bar{\Gamma}$-$\bar{K}$ direction, and $m^* = 0.3 m_e$ for the $\bar{\Gamma}$-$\bar{M}$ direction. Furthermore, the bottoms of the parabola totally changed from sample to sample in our STM measurements, though they are always located above E_F. Their values are (1.2 ± 0.1) eV and (0.21 ± 0.04) eV above E_F for the curves with squares and circles, respectively, in Fig. 4(b). These reasons will be discussed later.

In our STM observations, we obtained the images of two

types of OPB's as indicated by arrows *(A)* and *(B)* in Fig. 3, where the empty states were probed with the bias 1.0 V. Standing wave patterns can be seen near the protruded OPB indicated by *(A)* while the waves cannot be seen near the hollowed OPB indicated by *(B)*. The protruded one works as a potential barrier for electrons in the surface state; electrons are reflected by it, which contributes to making the standing waves. But the hollowed OPB does not work as a barrier. Electrons can pass through this type of boundary without reflection, and there are no observable standing waves.

Since our image corresponds to the empty states of the surface, the protruded OPB *(A)* is identical to type-I OPB in Ref. 13, but the hollowed one *(B)* is not. Considering that the hollowed one *(B)* is aligned along the $\langle 11\bar{2} \rangle$ directions, and always straight, it is not type-II OPB in Ref. 13 either. We made sure that the scanning direction of the STM tip did not matter for the difference of the protruded and hollowed ones.

To clarify the difference of the two OPB's, we scanned smaller regions, and investigated the arrangement of the bright spots near the boundaries in detail. There are two ways to shift the phase of the superstructure between the adjacent out-of-phase domains. An OPB along the $\langle 11\bar{2} \rangle$ direction can have a phase-shift vector of $\mathbf{d}_A = (\mathbf{a} - \mathbf{b})/3$ (which we call type-IA hereafter) or a phase-shift vector of $\mathbf{d}_B = -(\mathbf{a} - \mathbf{b})/3$ (which we call type-IB), where $\mathbf{a}$ and $\mathbf{b}$ are the surface unit vectors of the $\sqrt{3} \times \sqrt{3}$ structure. In the previous reports performed at room temperatures,[13,14,16] only type-IA is considered, which is the most stable OPB. The protruded boundary *(A)* in our image corresponds to the type-IA boundary, and the hollowed boundary *(B)* corresponds to the type-IB boundary.

Though the two types of boundaries are classified correctly, it is still unknown why the difference in making the standing waves occurs. Considering that the protrusion of type-IA boundary in STM image does not come from topography but some electronic state, it is possible that some particular electronic state, which is inherent only in the type-IA boundary is important for scattering and reflecting the surface-state electrons. But this is just an inference, and more investigations are required.

We should discuss here several other points about our standing wave observations; why can we obtain the wave patterns in conventional STM mode with bias voltages as high as around 1 V? Do the standing waves mean a metallic nature of the surface? And why are the dispersion relations obtained from the standing waves different from photoemission measurements?

When a bias voltage V is applied across the tunneling gap, all the density of states (DOS) between E_F and $E_F + eV$ contribute to the tunneling current superimposed with the weighted barrier-transmission coefficient. The wavelength of the standing wave should be different from energy to energy, so the smaller energy range of the superimposition of the local DOS is, the larger the amplitude of the standing wave observed in STM mode becomes, because one can avoid smearing out of different wavelengths. In previous reports,[1–4] low bias voltages (less than about 0.1 V) were actually applied to get the wave patterns clearly in conventional STM mode. To get the (energy-resolved) wave pat-

terns at higher bias voltages, STS (scanning tunneling spectroscopy) mode was adopted (mapping the differential conductance dI/dV).

However, we could actually observe standing waves at bias voltages as high as around 1 V in conventional STM mode (not in STS mode), and furthermore, their wavelengths actually changed depending on the bias voltages. This is because the oscillations of the standing waves in conventional STM images are determined by the particular wavelengths as described below. When the bottom of the energy dispersion curve is located above E_F, only the wave number k_0 corresponding to the energy level $E_F + eV$ determines the form of the oscillation. In case of a single straight step on an extended surface, the oscillating part of the tunneling current can be approximated by a sum of the two terms of the Bessel functions, $J_1(2k_0x)/(k_0x)$ and $J_2(2k_0x)/(k_0x)^2$ with appropriate coefficients, where x is a distance away from the step [see Eqs. (31) and (32) in Ref. 17]. Because enough of the smaller coefficient of the latter term compared with that of the first term and the faster decaying factor x^{-2}, the term $J_2(2k_0x)/(k_0x)^2$ can be neglected, and only the term $J_1(2k_0x)/(k_0x)$ remains. We also calculated the tunneling current by the integral of the density of states weighted by the barrier-transmission coefficient [Eq. (20) in Ref. 17] numerically, and checked this validity. So, we can say that the wavelengths of the observed standing waves in conventional STM images directly correspond only to the energy level $E_F + eV$ determined by the bias voltage V. But the oscillation $J_1(2k_0x)/(k_0x)$ in tunneling current decays faster than that of the differential conductance, which is given by the zeroth-order Bessel function. The wavelengths observed in the circular domain in Fig. 1(a) are almost equal to those near the straight steps shown in Fig. 1(a). Moreover, there seems no indication of quantization in the circular domain. So, we assumed that the discussion described above can be applied to the circular domain in Fig. 1(a) as well as straight steps and domain boundaries.

The next point to be discussed is the electronic structure of the $\sqrt{3} \times \sqrt{3}$-Ag surface itself. The standing waves previously observed on metal surfaces at very low-bias voltages[1–4] directly mean the existence of the Fermi surface, i.e., a metallic nature of electronic states. So, do our standing waves also indicate the metallic character of the $\sqrt{3} \times \sqrt{3}$-Ag surface? According to photoemission spectroscopy[10–12] and STS,[18] the $\sqrt{3} \times \sqrt{3}$-Ag surface is known to have an upward parabolic surface-state band crossing E_F, meaning a metallic nature. But our standing waves were observed in the local density of empty states well above E_F, and the bottoms of the dispersion curves fitted to the experimental data [Fig. 4(b)] seem to locate above E_F. Therefore, our standing waves do not necessarily indicate the metallic nature of the surface. Theoretical calculations actually showed an energy gap around E_F in the surface-electronic states.[9,19]

However, we cannot make a definite conclusion at the moment that the surface is semiconducting, because we could not obtain any STM images with bias voltages smaller than about 0.3 V at 6 K, which prevented us from probing the states near E_F. Furthermore, the minimum bias voltage for observing the waves was different from sample to sample, which caused the uncertainty in the bottom of the parabola mentioned at Fig. 4(b). This phenomenon is not due to a voltage drop along the Si crystal between the observed area and an electrode at the end clamp (about 5 mm long) with currents of nA range, because our Si wafer was a highly B-doped one so that it did not become insulating even at 6 K. So, we need other reasons why small bias voltage did not work and why the minimum bias voltage to get the images differed from sample to sample at 6 K. It might be caused by a Schottky barrier at the end clamp (between the Si crystal and Mo electrode) or some kind of charging-up effect due to a slow transfer rate of electrons from the surface state to the bulk states in Si at low temperature.

We also considered tip-induced band bending as another reason for this uncertainty in bias voltages. The surface states can work to screen the electronic field from the tip to reduce the electric field penetrating into the bulk, and decrease the band bending induced by the tip. In order to estimate the upper limit of the tip-induced band bending, we assumed the metal-insulator(vacuum)-semiconductor structure without surface (interface) states, and calculated the band bending numerically using a model in Ref. 20 with parameters for our p-type Si wafer. When the sample was negatively biased, the degree of the induced band bending was severe, almost equal to the bias voltage. On the other hand, when positively biased, there was little band bending, less than 0.015 V. This is because the concentration of holes in the bulk is large enough while that of electrons is nearly zero. Thus there is little effect of tip-induced band bending in empty-state imaging, and we can safely say that the value of the effective mass m^*, about $(0.13 \pm 0.04)m_e$, obtained from the dispersion curve in Fig. 4(b) is not affected by the tip-induced band bending, though there is an uncertainty in respect of the bottom energy of the curves.

This may also explain why the standing waves were not observed in filled-state images, even if the bottom of the free-electron-like surface state assumed to locate below E_F. The tip-induced band bending is so large in probing the filled states that scanning of the tip may cause local band bending dynamically, the probed states would be severely disturbed, and small oscillations of the standing waves would be buried in the large variation of the band bending, though we have not yet confirmed this on n-type samples experimentally. According to Ref. 21, the bottom of the surface-state band lies close to the valence-band maximum of the bulk Si. So, the electrons tunneled from the bulk states of the sample may dominate the electrons from the surface states, which may reduce the amplitude of the standing waves in the filled state. This might be another reason for preventing us from imaging the standing waves in the filled states.

Previous reports of photoemission spectroscopy[10–12] and STS (Ref. 18) of this surface were only at room temperature where it was suggested that dilute gas phase of Ag adatoms on top of the $\sqrt{3} \times \sqrt{3}$-Ag surface exist as a (meta)stable thermodynamical state, and that they donate electrons into the surface-state band, resulting in a metallic nature.[22] But at 6 K, such a doping effect might disappear to return the surface semiconducting, because the gas phase on top of the surface will condense into clusters to diminish the charge transfer into the substrate. Compared to the rather straight steps in the STM images taken at RT,[13] the steps in the STM images taken at 70 K (Ref. 23) or 6 K in the present paper

seem to be decorated by the condensed Ag clusters. To confirm this idea, photoemission spectroscopy or STS are required at low temperatures.

The effective mass $(0.13\pm0.04)\, m_e$ estimated from the standing waves is different from that obtained from photoemission spectroscopy $0.25 m_e$ (Ref. 10) as mentioned before. This discrepancy might come from the following reasons.

(1) The measured regions in k space are different between the two measurements; the photoemission probed a region near the bottom of the band (between 0.02 and $0.15\,\text{Å}^{-1}$ in wave number), while the present STM study probes far from the bottom (from 0.07 to $0.22\,\text{Å}^{-1}$). Therefore, if the dispersion curve deviates from a parabola, the two measurements will give different values of the effective mass.

(2) The sizes of probed area on the surface are quite different between the two measurements. The photoemission gives the values averaged over macroscopic areas on the surface, which inevitably include the effect of carrier scattering at step edges, domain boundaries, and other defects, leading to larger effective masses obtained. Such masses may be different from those obtained from the standing waves on terraces.

(3) The sample temperatures are different. We have recently found that another stable phase of the $\sqrt{3}\times\sqrt{3}$-Ag surface at low temperatures, which seems slightly different from the well-known HCT structure at RT. Its details will be published elsewhere. Therefore, the effective mass obtained at low temperatures can be different from that at RT.

The electron standing waves presented here, which indicate severe carrier scattering at step edges and domain boundaries, may be expected ones by considering a low-carrier mobility estimated from the surface-state conductivity on this surface.[22]

[1] M. F. Crommie, C. P. Lutz, and D. M. Eigler, Nature (London) **363**, 524 (1993); Science **262**, 218 (1993); M. F. Crommie, C. P. Lutz, D. M. Eigler, and E. J. Heller, Surf. Rev. Lett. **2**, 127 (1995); Physica D **83**, 98 (1995).

[2] Y. Hasegawa and Ph. Avouris, Phys. Rev. Lett. **71**, 1071 (1993); Ph. Avouris, I.-W. Lyo, R. E. Walkup, and Y. Hasegawa, J. Vac. Sci. Technol. B **12**, 1447 (1994).

[3] D. Fujita, K. Amemiya, T. Yakabe, H. Nejoh, T. Sato, and M. Iwatsuki, Phys. Rev. Lett. **78**, 3904 (1997).

[4] P. T. Sprunger, L. Petersen, E. W. Plummer, E. Lægsgaard, and F. Besenbacher, Science **275**, 1764 (1997).

[5] M. Schmid, W. Hebenstreit, P. Varga, and S. Crampin, Phys. Rev. Lett. **76**, 2298 (1996).

[6] M. C. M. M. van der Wielen, A. J. A. van Roij, and H. van Kempen, Phys. Rev. Lett. **76**, 1075 (1996).

[7] T. Takahashi and S. Nakatani, Surf. Sci. **282**, 17 (1993).

[8] M. Katayama, R. S. Williams, M. Kato, E. Nomura, and M. Aono, Phys. Rev. Lett. **66**, 2762 (1991).

[9] S. Watanabe, M. Aono, and M. Tsukada, Phys. Rev. B **44**, 8330 (1991).

[10] X. Tong, C.-S. Jiang, and S. Hasegawa, Phys. Rev. B **57**, 9015 (1998).

[11] L. S. O. Johansson, E. Landemark, C. J. Karlsson, and R. I. G. Uhrberg, Phys. Rev. Lett. **63**, 2092 (1989); **69**, 2451 (1992).

[12] S. Hasegawa, X. Tong, C.-S. Jiang, Y. Nakajima, and T. Nagao, Surf. Sci. **386**, 322 (1997).

[13] D. W. McComb, R. A. Wolkow, and P. A. Hackett, Phys. Rev. B **50**, 18 268 (1994).

[14] D. W. McComb, D. J. Moffatt, P. A. Hackett, B. R. Williams, and B. F. Mason, Phys. Rev. B **49**, 17 139 (1994).

[15] K. J. Wan, X. F. Lin, and J. Nogami, Phys. Rev. B **47**, 13 700 (1993).

[16] T. Nakayama, S. Watanabe, and M. Aono, Surf. Sci. **344**, 143 (1995).

[17] G. Hörmandinger, Phys. Rev. B **49**, 13 897 (1994).

[18] H. H. Weitering and J. M. Carpinelli, Surf. Sci. **384**, 240 (1997).

[19] Y. G. Ding, C. T. Chan, and K. M. Ho, Phys. Rev. Lett. **67**, 1454 (1991); **69**, 2452 (1992).

[20] S. M. Sze, *Physics of Semiconductor Devices,* 2nd ed. (Wiley, New York, 1981), pp. 362–379.

[21] J. Viernow, M. Henzler, W. L. O'Brien, F. K. Men, F. M. Leibsle, D. Y. Petrovykh, J. L. Lin, and F. J. Himpsel, Phys. Rev. B **57**, 2321 (1998).

[22] Y. Nakajima, S. Takeda, T. Nagao, S. Hasegawa, and X. Tong, Phys. Rev. B **56**, 6782 (1997).

[23] X. Tong, Y. Sugiura, T. Nagao, T. Takami, S. Takeda, S. Ino, and S. Hasegawa, Surf. Sci. **408**, 146 (1998).